TMA4212 - NUMDIFF

Project 2

Authors:
Lars Vatten, Jakob Heide, Celine Olsson

26.02.23

Table of Contents

Introduction

In this project we want to solve a 1d stationary convection diffusion problem. This can for instance be the transport/decay/ mixing of a chemical in a fluid moving in a finite tube. Our model is formulated as a Poisson like equation:

$$-\partial_x(\alpha(x)\partial_x u) + \partial_x(b(x)u) + c(x)u = f(x) \qquad \text{in } \Omega = (0,1) \tag{1}$$

where $\alpha(x) > 0$ is the diffusion coefficient, $b(x)$ is the fluid velocity, $c(x) \geq 0$ is the decay rate of the substance, u is the concentration of the substance and $f(x)$ is a source term.

Part 1

For this part we assume that $\alpha(x) \geq \alpha_0 > 0$, $c > 0$, $||\alpha||_{L^\infty} + ||b||_{L^\infty} + ||c||_{L^\infty} + ||f||_{L^2} \leq K$, and we will use Dirichlet boundary conditions, $u(0) = 0 = u(1)$.

a) Weak formulation of the problem

We first want to show that any classical solution u of this problem satisfies

$$a(u,v) = F(v) \quad \forall\ v \in V = H_0^1(0,1) \tag{V}$$

We start by taking equation (1) and multiplying it by a test function $v(x) \in H_0^1(0,1)$, so $v(0) = 0 = v(1)$, and then integrate over the domain Ω.

$$\int_0^1 -\partial_x(\alpha(x)\partial_x u)v\,dx + \int_0^1 \partial_x(b(x)u)v\,dx + \int_0^1 c(x)uv\,dx = \int_0^1 f(x)v\,dx$$

Using integration by parts we get a simplified equation:

$$\int_0^1 (\alpha u_x v_x - buv_x + cuv)\,dx = \int_0^1 fv\,dx \qquad \forall\ v \in H_0^1(0,1)$$

We denote the left hand side as $a(u,v)$ and the right hand side as $F(v)$.

For later use, we want to check if $a(u,v)$ and $F(v)$ has certain properties. This includes bilinearity, continuity and coerciveness for $a(u,v)$, and linearity and continuity for $F(v)$.

For $a(u,v)$ to be bilinear we need the following two conditions to be fulfilled:

$$a(c_1u_1 + c_2u_2, v) = c_1a(u_1,v) + c_2a(u_2,v) \tag{I}$$
$$a(u, c_1v_1 + c_2v_2) = c_1a(u,v_1) + c_2a(u,v_2) \tag{II}$$

$$\begin{aligned} a(c_1u_1 + c_2u_2, v) &= c_1\int_0^1 \alpha(u_1)_x v_x - bu_1v_x + cu_1v\,dx + c_2\int_0^1 \alpha(u_2)_x v_x - bu_2v_x + cu_2v\,dx \\ &= c_1a(u_1,v) + c_2a(u_2,v) \\ a(u, c_1v_1 + c_2v_2) &= c_1\int_0^1 \alpha u_x(v_1)_x - bu(v_1)_x + cuv_1\,dx + c_2\int_0^1 \alpha u_x(v_2)_x - bu(v_2)_x + cuv_2\,dx \\ &= c_1a(u_1,v) + c_2a(u_2,v) \end{aligned}$$

We see that both (I) and (II) holds, showing that $a(u,v)$ is bilinear.

Furthermore, we show that $a(u,v)$ is continuous. We use the result that a linear operator on a Banach space is continuous if it is bounded. Since H^1 is a Banach space, this theorem applies. We start by taking the absolute value:

$$|a(u,v)| = |\int_0^1 (\alpha u_x v_x - buv_x + cuv)dx|.$$

We bound this by moving the absolute value inside the integral, and use the triangle inequality on the integrand:

$$\begin{aligned}|a(u,v)| &\leq \int_0^1 |\alpha u_x v_x| dx + \int_0^1 |-buv_x| dx + \int_0^1 |cuv| dx \\ &= \int_0^1 |\alpha||u_x||v_x| dx + \int_0^1 |b||u||v_x| dx + \int_0^1 |c||u||v| dx\end{aligned}$$

We find a stricter bound by bounding the diffusion, convection and decay functions by the L^∞ norm. We pull these out of the integrals, and use Cauchy-Schwarz inequality to bound the remaining integrals further:

$$\begin{aligned}|a(u,v)| &\leq ||\alpha||_{L^\infty} \left(\int_0^1 |u_x|^2 dx\right)^{\frac{1}{2}} \left(\int_0^1 |v_x|^2 dx\right)^{\frac{1}{2}} + ||b||_{L^\infty} \left(\int_0^1 |u|^2 dx\right)^{\frac{1}{2}} \left(\int_0^1 |v_x|^2 dx\right)^{\frac{1}{2}} \\ &\quad + ||c||_{L^\infty} \left(\int_0^1 |u|^2 dx\right)^{\frac{1}{2}} \left(\int_0^1 |v|^2 dx\right)^{\frac{1}{2}} \\ &= ||\alpha||_{L^\infty} ||u_x||_{L^2} ||v_x||_{L^2} + ||b||_{L^\infty} ||u||_{L^2} ||v_x||_{L^2} + ||c||_{L^\infty} ||u||_{L^2} ||v||_{L^2}\end{aligned}$$

We know that since the H^1 norm of a function f is defined as the square root of the squared L^2 norm of the 0th and 1st derivative of f, the H^1 is a bound for the L^2 norm of both f and the first derivative of f. Hence we obtain a stricter bound by replacing the L^2 norms of u and u_x by the H^1 norm of u, and the same for v and v_x:

$$\begin{aligned}|a(u,v)| &\leq ||\alpha||_{L^\infty} ||u||_{H^1} ||v||_{H^1} + ||b||_{L^\infty} ||u||_{H^1} ||v||_{H^1} + ||c||_{L^\infty} ||u||_{H^1} ||v||_{H^1} \\ &= \left(||\alpha||_{L^\infty} + ||b||_{L^\infty} + ||c||_{L^\infty}\right) ||u||_{H^1} ||v||_{H^1} \\ &\leq K ||u||_{H^1} ||v||_{H^1} \end{aligned} \tag{2}$$

The last inequality is given by the bound on the sum of the L^∞ norm of the diffusion, convection and decay functions. In conclusion, since $a(u,v)$ is a bounded, linear function on a Banach space, it is also continuous.

In addition, we show that $F(v)$ is a linear and bounded functional on H_1. The linearity follows directly from the linearity of integrals,

$$F(c_1 v_1 + c_2 v_2) = \int_0^1 f(c_1 v_1 + c_2 v_2) dx = c_1 \int_0^1 f v_1 dx + c_2 \int_0^1 f v_2 dx = c_1 F(v_1) + c_2 F(v_2).$$

The continuity/boundedness of $F(v)$ can be showed using Cauchy-Schwarz inequality and the fact that $||.||_{L^2} \leq ||.||_{H^1}$,

$$|F(v)| = |\int_0^1 f v dx| \leq \int_0^1 |f||v| dx \leq \left(\int_0^1 |f|^2 dx\right)^{\frac{1}{2}} \left(\int_0^1 |v|^2 dx\right)^{\frac{1}{2}} = ||f||_{L^2} ||v||_{L^2} \leq ||f||_{L^2} ||v||_{H^1}.$$

b) Existence of a solution

Lastly we want to show that $a(u,v)$ is coercive. We start by proving that $a(u,v)$ satisfies the Gårding inequality,

$$a(u,u) \geq \left(\alpha - \frac{\epsilon}{2}|b|\right) \int_0^1 u_x^2 \, dx + \left(c - \frac{1}{2\epsilon}|b|\right) \int_0^1 u^2 \, dx, \tag{3}$$

which is shown below.

$$\begin{aligned}a(u,u) &= \int_0^1 \alpha u_x^2 - b u u_x + c u^2 \, dx \geq \int_0^1 \alpha u_x^2 - |b| \left(\frac{1}{2\epsilon} u^2 + \frac{\epsilon}{2} u_x^2\right) + c u^2 \, dx \qquad \text{(Young's inequality)} \\ &= \int_0^1 \alpha u_x^2 - |b| \frac{1}{2\epsilon} u^2 - |b| \frac{\epsilon}{2} u_x^2 + c u^2 \, dx = \int_0^1 \left(\alpha - \frac{\epsilon}{2}|b|\right) u_x^2 \, dx + \int_0^1 \left(c - \frac{1}{2\epsilon}|b|\right) u^2 \, dx\end{aligned}$$

We see above that the inequality holds, but only as long as b has a positive contribution (hence the absolute value), guaranteeing that the second term has a negative contribution.

We now use the Gårding inequality (3) to prove that $a(u,v)$ is coercive when $c > \frac{|b|^2}{2\alpha}$. For $a(u,v)$ to be coercive, it must satisfy

$$a(v,v) \geq M||v||_V^2 \quad \forall\ v \in V,$$

where M is the coercivity constant.

We start by rewriting the Gårding inequality.

$$a(u,u) \geq \left(\alpha - \frac{\epsilon}{2}|b|\right)\int_0^1 u_x^2\,dx + \left(c - \frac{1}{2\epsilon}|b|\right)\int_0^1 u^2\,dx = \left(\alpha - \frac{\epsilon}{2}|b|\right)||u_x||_{L^2}^2 + \left(c - \frac{1}{2\epsilon}|b|\right)||u||_{L^2}^2$$

Since this holds for all $\epsilon > 0$, we can set $\epsilon = \frac{\alpha}{|b|}$, giving us

$$\left(\alpha - \frac{\epsilon}{2}|b|\right)||u_x||_{L^2}^2 + \left(c - \frac{1}{2\epsilon}|b|\right)||u||_{L^2}^2 = \left(\frac{\alpha}{2}\right)||u_x||_{L^2}^2 + \left(c - \frac{|b|^2}{2\alpha}\right)||u||_{L^2}^2,$$

which is greater than zero when $c > \frac{|b|^2}{2\alpha}$. If we denote $M = \min\{\frac{\alpha}{2}, c - \frac{|b|^2}{2\alpha}\}$, we get the following inequality:

$$a(u,u) \geq \left(\frac{\alpha}{2}\right)||u_x||_{L^2}^2 + \left(c - \frac{|b|^2}{2\alpha}\right)||u||_{L^2}^2 \geq M||u||_{H^1}^2 = M||u||_V^2 \tag{4}$$

The last equation comes from the fact that $V = H_0^1(0,1)$. We see that the coercivity only holds as long as $c > \frac{|b|^2}{2\alpha}$.

Part 2

We now want to solve (V) with $\mathbb{P}_1$ FEM on a general grid on $(0,1)$:

$$\text{find } u \in V_h \text{ s.t. } \ a(u_h, v_h) = F(v_h) \quad \forall\ v_h \in V_h = X_h^1(0,1) \cap H_0^1(0,1) \tag{V_h}$$

We let $\alpha \geq 0$, b and $c \geq 0$ be non-zero constants.

In this section, we implement the $\mathbb{P}_1$ FEM and test it numerically. We define our test function space V_h as $V_h = X_h^1(0,1) \cap H_0^1(0,1)$, i.e. the space of piecewise linear functions on the interval $[0,1]$ that are 0 at the boundaries $x = 0$ and $x = 1$. The basis of this space $\{\phi_i\}_{i=0}^M$ is the set of hat functions corresponding to the nodes in the triangulation given by the grid. More mathematically, the basis functions are defined as $\phi_i(x)$ on the inner nodes, and $\phi_0(x)$ and $\phi_M(x)$ on the edge nodes:

$$\phi_i(x) = \begin{cases} \frac{x - x_i}{x_i - x_{i-1}}, & x \in [x_{i-1}, x_i) \\ \frac{x_{i+1} - x_i}{x_{i+1} - x_i}, & x \in [x_i, x_{i+1}] \\ 0, & \text{else} \end{cases} \quad \phi_0(x) = \begin{cases} \frac{x_1 - x}{x_1}, & x \in [0, x_1] \\ 0, & \text{else} \end{cases} \quad \phi_M(x) = \begin{cases} \frac{x - x_{M-1}}{1 - x_{M-1}}, & x \in [x_{M-1}, 1] \\ 0, & \text{else} \end{cases}$$

The derivatives of the basis functions is needed to compute the stiffness matrix in the FEM, and are given as $\phi_i'(x)$ on the inner nodes, and $\phi_0'(x)$ and $\phi_M'(x)$ on the edges:

$$\phi_i'(x) = \begin{cases} \frac{1}{x_i - x_{i-1}}, & x \in [x_{i-1}, x_i) \\ -\frac{1}{x_{i+1} - x_i}, & x \in [x_i, x_{i+1}] \\ 0, & \text{else} \end{cases} \quad \phi_0'(x) = \begin{cases} -\frac{1}{x_1}, & x \in [0, x_1] \\ 0, & \text{else} \end{cases} \quad \phi_M'(x) = \begin{cases} \frac{1}{1 - x_{M-1}}, & x \in [x_{M-1}, 1] \\ 0, & \text{else} \end{cases}$$

a) Implementation

Before we set up the implementation in Python, we must do some preparatory analytical work. In particular, we calculate the elements of the stiffness matrix A by hand. The elements of the stiffness matrix is given as

$$a_{ij} = a(\phi_i, \phi_j) = \int_0^1 \left(\alpha\phi_{i,x}\phi_{j,x} + b\phi_i\phi_{j,x} + c\phi_i\phi_j\right)dx.$$

We observe that, by the definition of the hat functions, a product $\phi_i(x)\phi_j(x)$ is non-zero only if $i = j$ or $i = j \pm 1$. Hence our stiffness matrix will be a tridiagonal matrix. Since each hat function is piecewise defined to be non-zero only on two specific intervals and 0 elsewhere, the product $\phi_i(x)\phi_j(x)$ is a piecewise function which gives rise to 5 different cases on the domain; non-zero on 4 specific intervals and 0 elsewhere. The same is the case for the products $\phi_i(x)\phi_j'(x)$ and $\phi_i'(x)\phi_j'(x)$. The expressions to consider for the integration are

$$\phi_i(x)\phi_j(x) = \begin{cases} \frac{(x-x_{i-1})^2}{h_i^2}, & x \in K_i = K_j \\ \frac{(x-x_{i-1})(x_i-x)}{h_i^2}, & x \in K_i = k_{j+1} \\ \frac{(x_{i+1}-x)(x-x_i}{h_{i+1}^2}, & x \in K_{i+1} = K_j \\ \frac{(x_{i+1}-x)^2}{h_{i+1}^2}, & x \in K_{i+1} = K_{j+1} \\ 0, & \text{elsewhere} \end{cases} \qquad \phi_i(x)\phi_j'(x) = \begin{cases} \frac{x-x_{i-1}}{h_i^2}, & x \in K_i = K_j \\ -\frac{x-x_{i-1}}{h_i^2}, & x \in K_i = k_{j+1} \\ \frac{x_{i+1}-x}{h_{i+1}^2}, & x \in K_{i+1} = K_j \\ -\frac{x_{i+1}-x}{h_{i+1}^2}, & x \in K_{i+1} = K_{j+1} \\ 0, & \text{elsewhere} \end{cases}$$

$$\phi_i'(x)\phi_j'(x) = \begin{cases} \frac{1}{h_i^2}, & x \in K_i = K_j \\ -\frac{1}{h_i^2}, & x \in K_i = k_{j+1} \\ -\frac{1}{h_{i+1}^2}, & x \in K_{i+1} = K_j \\ \frac{1}{h_{i+1}^2}, & x \in K_{i+1} = K_{j+1} \\ 0, & \text{elsewhere} \end{cases},$$

where we have written $x_i - x_{i-1}$ as h_i and the interval $[x_{i-1}, x_i)$ as element K_i. Carrying out the integration, we find that the elements in the stiffness matrix A are given by

$$a_{ij} = \begin{cases} -\frac{\alpha}{h_{i+1}} + \frac{1}{2}b + \frac{1}{6}ch_{i+1}, & i = j-1 \\ \alpha(\frac{1}{h_i} + \frac{1}{h_{i+1}}) + \frac{1}{3}ch_i, & i = j \\ -\frac{\alpha}{h_i} - \frac{1}{2}b + \frac{1}{6}ch_i, & i = j+1 \end{cases}.$$

Furthermore, we compute the elements F_i of the right hand side through numerical integration on each component,

$$F_i = \int_0^1 f(x)\phi_i(x)dx \approx Q(f\phi_i, [0,1]),$$

where Q denotes some numerical quadrature formula of sufficient order (sufficient in the sense that it does not interfere with the order of FEM, which is order 2.). In our implementation, scipy's `integrate.quad()` function is used to integrate the right hand side, which uses a fixed-tolerance Gaussian quadrature method.

We test our implementation with a test solution u_1, and calculate the corresponding f_1 from equation (1):

$$u_1 = \sin(10\pi x)\ , \qquad f_1 = 100\alpha\pi^2 \sin(10\pi x) + 10b\pi\cos(10\pi x) + c\sin(10\pi x)$$

We use the nodes $x = \big(0.0\ 0.016\ 0.146\ 0.18\ 0.219\ 0.348\ 0.497\ 0.531\ 0.7\ 0.737\ 0.984\ 1.0\big)$, which are randomly spaces in our domain. α, b and c are set to be equal to 1. Figure 1 shows the stiffness matrix corresponding to this set of nodes.

The numerical solution using u_1, f_1 and x from our FEM implementation is shown in Figure 2. The numerical solution looks to be a good approximation, but we want a quantitative measure of the precision of the method.

70.24	-7.17	0	0	0	0	0	0	0	0
-8.17	37.16	-28.91	0	0	0	0	0	0	0
0	-29.91	55.08	-25.13	0	0	0	0	0	0
0	0	-26.13	33.45	-7.23	0	0	0	0	0
0	0	0	-8.23	14.56	-6.19	0	0	0	0
0	0	0	0	-7.19	36.18	-28.91	0	0	0
0	0	0	0	0	-29.91	35.4	-5.39	0	0
0	0	0	0	0	0	-6.39	33.01	-26.52	0
0	0	0	0	0	0	0	-27.52	31.17	-3.51
0	0	0	0	0	0	0	0	-4.51	66.64

Figure 1: Stiffness matrix for one set of nodes

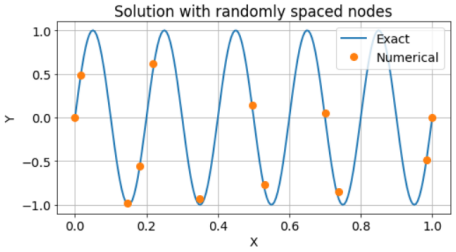

Figure 2: Solution for one set of nodes

b) Convergence in H^1 and L^2

In this section we investigate the convergence of the method. We test our implementation on the two analytical solutions

$$u_1(x) = \sin(10\pi x) \qquad \text{and} \qquad u_2(x) = x(1-x).$$

We compute the numerical solutions with equidistant grid points, and compare the results as we increase the number of nodes in the triangulation. We start with a triangulation of 20 nodes, and double the number of nodes for each iteration, with 5 iterations in total. We compute the order of convergence and plot the error, measured in both the L^2-norm and H^1-norm. In addition we plot the theoretical error bound in H^1, which we derived in class as

$$\|u - u_h\|_{H^1} \leq \frac{2K}{M}\|u''\|_{L^2} h$$

The results can be seen in figure (3).

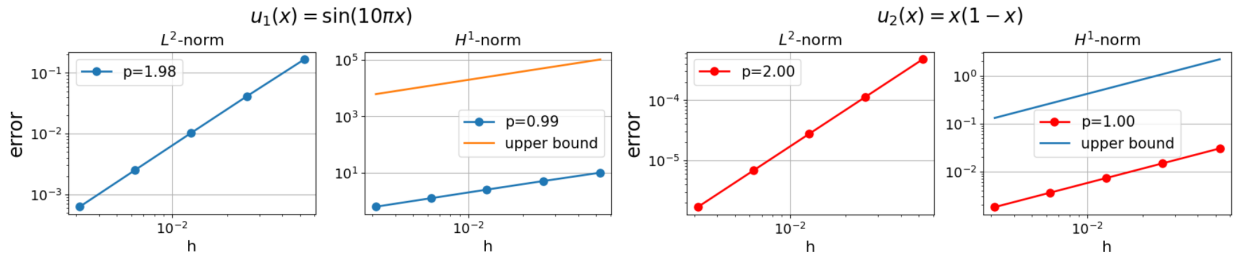

Figure 3: Convergence plots for u_1 and u_2.

We observe that the order of convergence is 2 for both solutions when measuring the error in the L^2-norm, and 1 for both solutions when measuring the error in the H^1-norm. The error varies between around 10^{-3} and 10^{-1} in the L^2-norm and around 10^0 and 10^1 in the H^1-norm for u_1. For u_2, the error varies between around 10^{-6} and 10^{-3} in the L^2 norm, and around 10^{-3} and 10^{-1} in the H^1-norm. The error in u_1 is probably larger because it is a rapidly changing function with many oscillations on the interval.

c) Galerkin orthogonality, Cea's lemma

In this section we aim to show Galerkin orthogonality for the $\mathbb{P}_1$ FEM, as well as showing that Cea's lemma holds for our problem.

The problem (V_h) is Galerkin orthogonal if for a solution u to the problem (V), and a solution u_h to the weak formulation (V_h), we have

$$a(u - u_h, v_h) = 0 \quad \forall\ v_h \in V_h \tag{5}$$

To prove this, we use the fact that $V_h \subset V$, and in equation (V) can choose a $v \in V_h$ and get

$$a(u, v_h) = F(v_h) \quad \forall\ v_h \in V_h$$

We use this in equation (5) to prove Galerkin orthogonality.

$$a(u - u_h, v_h) = a(u, v_h) - a(u_h, v_h) = F(v_h) - F(v_h) = 0$$

Since Lax-Milgram theorem is satisfied, Cea's lemma applies. It states that when we have u and u_h as solutions to (V) and (V_h) respectively, the following inequality holds:

$$||u - u_h||_V \leq \frac{K}{M}||u - v_h||_V \quad \forall\ v_h \in V_h \tag{6}$$

Here K is the continuity constant, and M is the coercivity constant.

We start with the coercivity property (4) for our problem with respect to the error $u - u_h$, with M as the coercivity constant.

$$M||u - u_h||_{H^1}^2 \leq a(u - u_h, u - u_h)$$

We then use that $u - u_h = u - v_h + v_h - u_h$.

$$M||u - u_h||_{H^1}^2 \leq a(u - u_h, u - v_h) + a(u - u_h, v_h - u_h) = a(u - u_h, u - v_h)$$

The last term comes from Galerkin orthogonality - since $v_h - u_h \in V_h$ the term $a(u - u_h, v_h - u_h)$ equals zero. Using the continuity property (2) we see that the last term can be written as

$$a(u - u_h, u - v_h) \leq K||u - u_h||_{H^1}||u - v_h||_{H^1},$$

where K is the continuity constant. When dividing both sides by $||u - u_h||_{H^1}$ and moving M to the right hand side, we get the inequality

$$||u - u_h||_{H^1} \leq \frac{K}{M}||u - v_h||_{H^1}.$$

Since $V = H_0^1(0, 1)$ the inequality above is equivalent to Cea's lemma (6).

Using Cea's lemma we can find a H^1 error bound:

$$||u - u_h||_{H^1} \leq \frac{K}{M} \inf_{v_h \in V_h} ||u - v_h||_{H^1} \leq \frac{2K}{M}||u''||_{L^2(0,1)} \cdot h$$

where we use that the interpolation error estimate in the H^1-norm is $\tilde{E}_h(v) \leq 2h||v''||_{L^2(0,1)}$. We see that the H^1 error bound is of first order, which corresponds with our results in section b). The theoretical H^1 error bound is plotted as the upper bound in Figure 3.

d) Non-smooth exact solutions

In this section, we explore the differentiability (in the weak sense) of a pair of non-smooth functions, and investigate how the non-smoothness affects numerical approximations in the $\mathbb{P}_1$ FEM. We recall the definition of the weak derivative. $g(x)$ is a weak derivative of $f(x)$ if the following conditions hold:

$$g(x) \in L^1(0, 1) \tag{I}$$

$$\int_0^1 gv = -\int_0^1 f\partial_x v, \ \forall v \in C^1(0, 1) \tag{II}$$

where $v(0) = 0 = v(1)$. We use this definition to check if there exists weak derivatives of our two non-smooth functions:

$$\omega_1(x) = \begin{cases} 2x, \ x \in (0, 1/2) \\ 2(1 - x), \ x \in (1/2, 1) \end{cases} \qquad \text{and} \qquad \omega_2(x) = x - |x|^{2/3}$$

Starting with $\omega_1(x)$, we consider the function $g_1(x) = \begin{cases} 2, \ x \in (0, 1/2) \\ -2, \ x \in (1/2, 1) \end{cases}$:

$$\int_0^1 |g_1(x)|dx = \int_0^{1/2} 2dx + \int_{1/2}^1 2dx < \infty$$

so (I) holds. For (II) we find, using integration by parts,

$$\begin{aligned} \int_0^1 g_1 v dx &= -\int_0^1 \omega_1 \partial_x v dx \\ \int_0^{1/2} 2v dx + \int_{1/2}^1 -2v dx &= -\int_0^{1/2} 2x\partial_x v dx - \int_{1/2}^1 2(1 - x)\partial_x v dx \\ &= -v\left(\frac{1}{2}\right) + \int_0^{1/2} 2v dx - \left(-v\left(\frac{1}{2}\right)\right) + \int_{1/2}^1 -2v dx \end{aligned}$$

This equation holds for any $v \in C_0^1(0,1)$, and (II) is satisfied - $g_1(x)$ is a weak derivative of $\omega_1(x)$. $g_1(x)$ is a scaled and translated Heaviside function, whose derivative is defined as the Dirac delta function. The Dirac delta function is not in L^2 and there is no second order weak derivative. Consider now the function $g_2(x) = 1 - \frac{2}{3(x)^{1/3}}$, $x \in \mathbb{R}\backslash\{0\}$. (I) holds since

$$\int_0^1 g_2(x)dx = 0 < \infty$$

and we can check (II) by

$$\int_0^1 g_2 v dx = -\int_0^1 \omega_2 \partial_x v dx$$

$$\int_0^1 (1 - \frac{2}{3x^{1/3}})v = -\int_0^1 (x - x^{2/3})\partial_x v dx = -[xv]_0^1 + \int_0^1 1v dx + [x^{2/3}v]_0^1 - \int_0^1 \frac{2}{3x^{1/3}}v = \int_0^1 g_2 v dx$$

so (II) holds - $g_2(x)$ is a weak derivative of ω_2. Consider now the function $h_2(x) = \frac{2}{9x^{4/3}}$. This function is not in L^1 since the integral $\int_0^1 h_2(x)dx$ diverges, and $h_2(x)$ can therefore not be a weak derivative of $g_2(x)$.

For $\omega_1(x)$ and $\omega_2(x)$ to be in $H^1(0,1)$, we require that $\omega_1(x), \omega_2(x), g_1(x), g_2(x) \in L^2$:

$$\int_0^1 |\omega_1(x)|^2 dx = \int_0^{1/2} 4x^2 dx + \int_{1/2}^1 4(1-x)^2 dx < \infty \qquad \int_0^1 |g_1(x)|^2 dx = \int_0^{1/2} 4dx + \int_{1/2}^1 4dx < \infty$$

$$\int_0^1 |\omega_2(x)|^2 dx = \int_0^1 |x - |x|^{2/3}|^2 dx = \frac{1}{84} < \infty \qquad \int_0^1 |g_2(x)|^2 dx = \frac{1}{3} < \infty$$

Hence $\omega_1(x), \omega_2(x) \in H^1(0,1)$, but not in $H^2(0,1)$ since there does not exist any second order weak derivatives.

We test the convergence of the FEM in H^1 and L^2 for the problems corresponding to these two solutions. When computing the right hand side F, we use the integration by parts formula to move one derivative from w_{xx} over to the test functions ϕ_i, such that the integrals we compute only contains (weak) derivatives that actually exist.

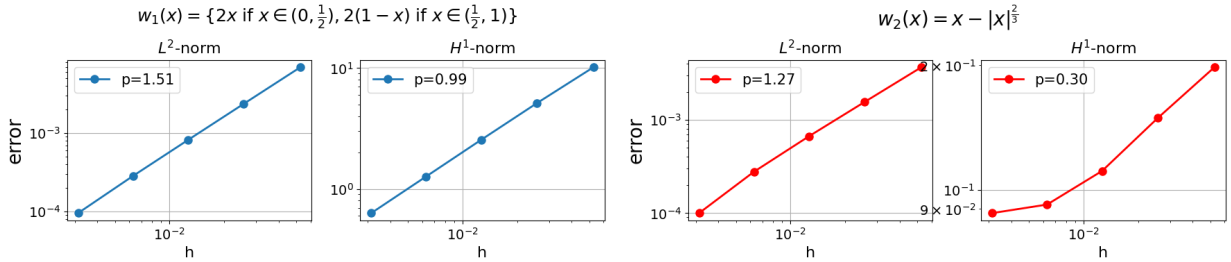

Figure 4: Convergence plots for w_1 and w_2

We observe that the order is indeed smaller than the order we obtained for the smooth functions we solved for in previous sections. In particular, we observe that the order is significantly lower in H^1 for w_2, which is reasonable since the derivative of w_2, which is included in the calculation of the H^1-norm, approaches infinity as x approaches zero. Plots of the numerical solutions along with the exact solutions can be found in appendix A1, figure 5.

e) Different positioning of nodes

We now want to check if the placement of the nodes has an impact on the accuracy and the error of the numerical solution. We consider the function:

$$f(x) = x^{-1/4} \qquad \text{for } x \in (0,1)$$

The function $f(x)$ is in $L^2(0,1)$ since the integral of its square is finite, as shown below.

$$\int_0^1 |f(x)|^2 \, dx = \int_0^1 x^{-1/2} \, dx = \left[2x^{1/2}\right]_0^1 = 2 < \infty$$

Two cases are considered - one case where there are more nodes closer together near $x = 0$, and another case where the nodes are equidistant. We use the same number of nodes in both cases. In the first case the nodes x_1 are used, and in the second case the nodes x_2 are used (see A2 and A3).

Since we do not know the exact solution, we create a numerical solution with a very refined grid as a reference solution. We want to find which case has the smallest error, measured in the L^2-norm.

If we keep the constants α, b and c to have the value 1, the difference between the reference solution and when more nodes are close to zero, is twice as big compared to the difference between the "exact" solution and the solution with the equidistant nodes (0.03509 vs 0.01755). This is as expected in this case, because the function is symmetric when $\alpha = b = c = 1$. The plot of this result can be seen in A2, Figure 6.

However if we now set $\alpha = 1$, $b = -10$ and $c = 4$, we get a non-symmetric function. The difference for the case of more nodes near zero is 0.00027, and 0.00094 for the case of equidistant nodes. The error is smaller when we move more nodes closer to $x = 0$ because the function grows rapidly in this area. The result of this can be seen in A3, Figure 7.

A1: Solutions for w_1 and w_2

[A1]

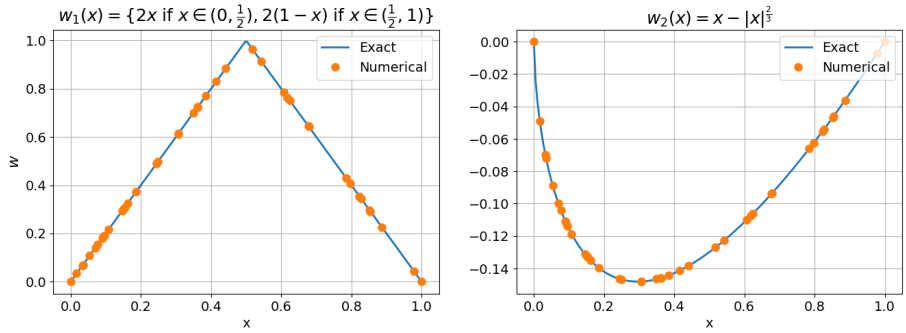

Figure 5: FEM approximations of w_1 and w_2.

A2: Solutions with differently spaced nodes, symmetric

$$\alpha = b = c = 1$$

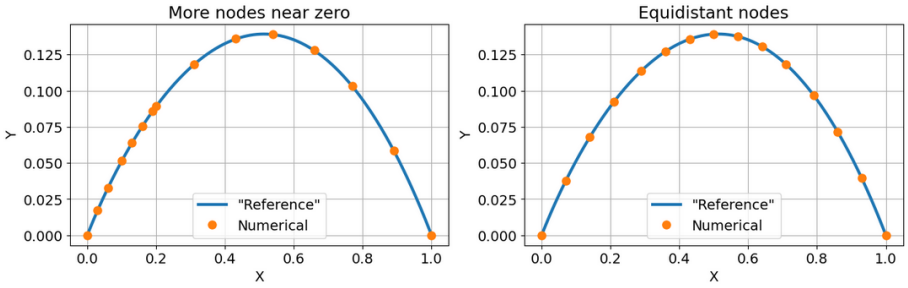

Figure 6: Solutions with differently spaced nodes

$x_1 = \big($0.0 0.03 0.06 0.1 0.13 0.16 0.19 0.2 0.31 0.43 0.54 0.66 0.77 0.89 1.0$\big)$
$x_2 = \big($0.0 0.07 0.14 0.21 0.29 0.36 0.43 0.5 0.57 0.64 0.71 0.79 0.86 0.93 1.0$\big)$.

A3: Solutions with differently spaced nodes, non-symmetric

$$\alpha = 1 \quad b = -10 \quad c = 4$$

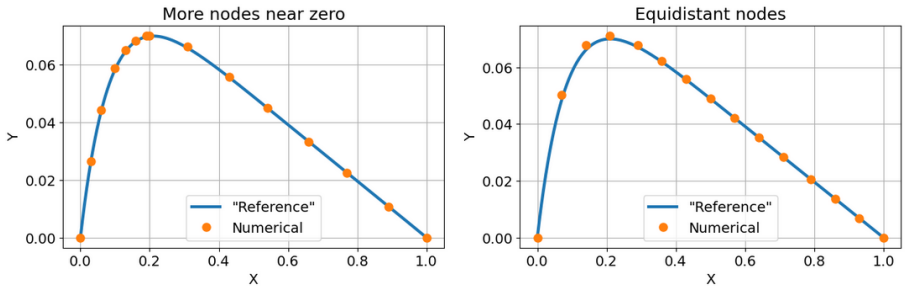

Figure 7: Solutions with differently spaced nodes

$x_1 = \big($0.0 0.03 0.06 0.1 0.13 0.16 0.19 0.2 0.31 0.43 0.54 0.66 0.77 0.89 1.0$\big)$
$x_2 = \big($0.0 0.07 0.14 0.21 0.29 0.36 0.43 0.5 0.57 0.64 0.71 0.79 0.86 0.93 1.0$\big)$.